Susceptibility and radiometry data used for stratigraphic correlations: case study on Upper Triassic beds in Turkey

SUSANNE MAYRHOFER* & ALEXANDER LUKENEDER

Geological-Palaeontological Department, Natural History Museum Vienna, Burgring 7, 1010 Vienna, Austria

**Corresponding author (e-mail: susanne.mayrhofer@nhm-wien.ac.at)*

Abstract: A Julian/Tuvalian (=Lower/Upper Carnian) substage boundary within the Kasımlar Formation, recently detected at Aşağiyaylabel (Taurus Mountains, Turkey) by facies analyses and biostratigraphic ammonoid investigations, was additionally detected by magnetic susceptibility (MS) and radiometry data. The Aşağiyaylabel sequence, a key section concerning environmental changes during Early to Late Carnian time, represents a deepening sequence from platform carbonates to pelagic limestones and marls. The Julian/Tuvalian boundary strata can be correlated over wide areas due to a positive shift in MS values from 11–105 $\times 10^{-6}$ SI (range AS I, KA IV) at the Lower Carnian sediments to 62–458 $\times 10^{-6}$ SI (range AS I, KA IV) at the Upper Carnian sediments as well as in radiometry values from 21.35–83.27 nGy h^{-1} (range AS I, KA IV) at the Lower Carnian sediments to 38.43–130.24 nGy h^{-1} (range AS I, KA IV) at the Upper Carnian sediments. A second, smaller positive shift in MS occurs at the transition from shallow-water carbonates of the Kartoz Formation (-11 to 71 $\times 10^{-6}$ SI; range AS I–KA II) into deeper-water carbonates from the base of the Kasımlar Formation (3–108 $\times 10^{-6}$ SI; range AS I–KA II). This study presents the first MS and radiometry data from Lower to Upper Carnian sediments. They reliably reflect lithological changes and display a direct function of enhanced terrigenous input into marine sediment systems, most probably caused by variations in climatic conditions.

The section AS I at Aşağiyaylabel (Taurus Mountains, Turkey), located within the Taurus Platform Units, comprises an Early to Late Carnian platform deepening sequence. It yields an ammonoid mass occurrence ('*Kasimlarceltites* acme zone'), deposited during the Early Carnian time (Upper Triassic), which is described from the whole Tethyan realm as an episode which saw the demise of reef and carbonate platforms (Tollmann 1976; Simms & Ruffell 1989; Riedel 1991; Aigner & Bachmann 1992; Hallam 1996; Hallam & Wignall 1997; Rüffer & Zamparelli 1997; Flügel & Senowbari-Daryan 2001; Keim *et al.* 2001; Hornung & Brandner 2005; Kozur & Bachmann 2010; Lukeneder *et al.* 2012).

The sudden deepening at AS I was apparently triggered by synsedimentary tectonics, which led to a new basin geometry along a deeper ramp setting, due to down-faulting and tilting of the platform (Lukeneder *et al.* 2012). Accordingly, the depositional environment at the northern Tethyan passive margin changed from a mid ramp over an outer ramp into a basinal position. Shallow-water carbonates from the Kartoz Formation were replaced by deeper-water limestones and marlstones of the Kasımlar Formation. A low-energy, bottom environment was interpreted based on the autochthonous fine-grained deeper-water limestones. Allochthonous biogenic material, for example, thick-shelled bivalves, gastropods and plasticlasts within the pelagic limestones, indicate episodic input of thin (several millimetres-thick) coarse-grained sediment layers from different source areas (proved by the microfacies; see Table 1) of the foreslope or shallow marine ramp (Lukeneder *et al.* 2012). The general deepening of the carbonate ramp at AS I is demonstrated by both the ammonoid biostratigraphy (Lukeneder & Lukeneder 2014) and the facies analysis (Lukeneder *et al.* 2012).

The Julian/Tuvalian boundary (=Lower/Upper Carnian boundary) is also clearly observable at AS I, as demonstrated by detailed facies analyses and ammonoid-biostratigraphic investigations (Lukeneder *et al.* 2012, Lukeneder & Lukeneder 2014). Correlatable sections in the vicinity of AS I represent similar sediment sequences, with somewhat different thickness. Due to the similarities in lithological units (e.g. shallow-water limestones, ammonoid beds, Julian/Tuvalian boundary) the distinct sections can be well correlated. These interpretations, based on facies and biostratigraphy, are strengthened by the magnetic susceptibility (MS) and radiometry values as exemplified in the present paper.

From: Da Silva, A. C., Whalen, M. T., Hladil, J., Chadimova, L., Chen, D., Spassov, S., Boulvain, F. & Devleeschouwer, X. (eds) *Magnetic Susceptibility Application: A Window onto Ancient Environments and Climatic Variations*. Geological Society, London, Special Publications, **414**, http://dx.doi.org/10.1144/SP414.10

Table 1. *Facies description of the different lithologies from Aşağiyaylabel (AS) and Karapinar (KA)*

Facies	Bed Thickness & Geometry					Biogenic Components	Rock-Classification
	AS I	AS IV	KA I	KA II	KA IV		
In situ corals	70 cm massive light-grey limestone	>1.8 m massive light-grey limestone				*in situ* corals, crinoids and rare ammonoids	Coral bafflestone
Shallow-water limestone	50 cm thick light-grey massive limestone	50–200 cm thick light-grey massive limestone	60 cm massive light-grey limestone bearing breccias	200 cm thick light-grey massive limestone		Abundant grains encrusted by cyanobacteria together with common megalodontid bivalves and echinoderm fragments	Bioclastic grainstone
Cipit-like boulders	8.1 m mixed carbonate blocks embedded within reworked material	8.1 m mixed carbonate blocks embedded within reworked material				Up to metre-sized patch reef blocks, Cipit boulders, small ammonoid-coquina and filaments,	Debris flow deposits
Bedded limestones with *Kasimlarceltites*	5–30 cm thick dark-grey limestone beds with wavy surface, stylolithic structures and calcite cleavages	5–45 cm thick dark-grey limestone beds with wavy surface	2–14 cm thick bedded dark-grey limestone beds with wavy surface	12–20 cm thick dark-grey limestone beds with wavy surface and calcite cleavage		Pelsparitic matrix	Pelagic wackestone/ ammonoid-floatstone
Bedded limestones with spherical bioturbation	4–60 cm thick bedded dark-grey limestone beds bearing spherical bioturbation and calcite cleavage				3–12 cm thick bedded dark-grey limestone beds bearing spherical bioturbation and yellowish residual crusts	Intercalations of fine-grained allodapic layers	Peloidal pack- to grainstone
Marly limestones	Tectonically fissile mm–cm laminated yellowish-grey marly limestones				tectonically fissile, mm–cm laminated yellowish-grey marly limestones		Bioclastic wackestone
Shales	Tectonically fissile (in the field of decimetre) brownish shales					Thin shelled bivalves, foraminifera, ammonoids, echinoderms and bioturbation	Argillaceous borrowed peloidal packstone

MS is explained as the induced magnetization which arises at minerals within a certain rock sample, brought into a low-strength magnetic field (Kodama 2012). It is one of numerous methods for detecting the properties of magnetic rocks. Such features are important in certain environments (Jovane *et al.* 2013). Since Robinson (1990), MS has become a standard technique for logging sediment cores. A number of additional authors have described a close relationship between the MS signature and the facies of marine environments (Devleeschouwer 1999; Ellwood *et al*. 2000; Zhang *et al.* 2000; Racki *et al.* 2002; Da Silva & Boulvain 2006; Babek *et al.* 2010; Lukeneder *et al.* 2010). This relationship is the result of erosion and weathering, caused by sea-level changes (regression/transgression; Crick *et al.* 1997, Ellwood *et al.* 1999) or by climatic changes (Crick *et al.* 2001, 2002). Whilst most studies concentrate on climate-driven cyclostratigraphic aspects (magnetosusceptibility event and cyclostratigraphy (MSEC); e.g. Crick *et al.* 1997; Ellwood *et al.* 2001, 2013*a*, 2013*b*; Whalen & Day 2010), regional events, caused by tempestites or storm events, can be also important for correlation and interpretation at a local scale. Furthermore, many studies measure MS by detailed rock sampling and subsequent highly sensitive laboratory measurements (e.g. Hladil *et al.* 2006).

In contrast to such highly sensitive measurements, the present study represents an 'averaging' method (Hladil *et al.* 2006) of MS and radiometry measurements. It compares the MS and radiometry data of the Upper Triassic section AS I from Aşağiyaylabel from the Taurus Mountains of Turkey (Anatolia) with four time-equivalent sections near Aşağiyaylabel (AS IV) and Karapinar (KA I–II & IV). The MS and radiometry values or peaks depict mineralogical and sedimentological variations. These variations can be directly used for straightforward correlations of time-equivalent sequences on a regional scale. MS and radiometry results should be interpreted with caution as trend-data. Nonetheless, the characteristic peaks at the Julian/Tuvalian boundary as well as at the lithological boundary between the shallow-water carbonates (Kartoz Formation) and deeper-water carbonates (Kasımlar Formation) help to localize these particular sequences at surrounding localities. These peaks form the basis of the detailed facies and biostratigraphic investigations undertaken in this study.

Geography and geology

Aşağiyaylabel and its surrounding sections are located in southern Turkey (Anatolia) about 90 km NE of Antalya and about 70 km SE of Isparta (Fig. 1a, b). The main section (AS I) crops out at the northern slope of an east–west-trending ridge, adjacent to the small village of Aşağiyaylabel (1050–1100 m above sea level, 37°33′05″N, 31°18′14″E). The second section (AS IV) is quite close, 0.5 km NW of AS I (37°55′47.9″N, 31°30′04.8″E; Fig. 1c). The village Karapinar (Fig. 1b) is about 2.8 km N–NW of Aşağiyaylabel, with its three sections KA I (37°57′69.2″N, 31°29′12.5″E), KA II (37°57′62.9″N, 31°29′20.5″E) and KA IV (37°57′69.9″N, 31°29′21.0″E; Fig. 1d). Geologically, both localities – Aşağiyaylabel and Karapinar – belong to the Taurus Platform Units, located within the Anamas Dağ, south of the Izmir-Ankara Suture and north of the Antalya Suture (Robertson 1993; Senel 1997; Andrew & Robertson 2002; Robertson *et al.* 2003; Lukeneder *et al.* 2012). The Anamas Dağ, or Anamas-Akseki Autochthonous, bears a Middle to Upper Triassic sequence of limestones, marlstones and shales that is up to 200 m thick (Gindl 2000). This sequence has already been investigated by Özgül & Arpat (1973), Dumont & Kerey (1975), Monod (1977), Poisson (1977), Gutnic *et al.* (1979), Robertson (1993, 2000), Senel (1997), and Robertson *et al.* (2003). During the Late Triassic, the Anatolian System and therefore the investigated sequences were part of microplates known as 'Cimmerian terranes' within the western Tethyan Ocean, located between the northern Palaeotethys and the southern Neotethys (Şengör *et al.* 1984; Scotese *et al.* 1989; Dercourt *et al.* 1993, 2000; Scotese 1998, 2001; Gindl 2000; Stampfli & Borel 2002; Stampfli *et al.* 2002; Gradstein *et al.* 2004). The subsequent subduction of the Palaeotethys under South Eurasia led to an extension of the Neotethys between Africa and the Cimmerian terranes. The sediments of today's Turkey were deposited on the western parts of the Cimmerian terranes.

The facies changes at Aşağiyaylabel (AS I and AS IV) and Karapinar (KA I–II & IV)

Aşağiyaylabel I (AS I). The main section at Aşağiyaylabel (AS I) consists of the Kartoz Formation and the Kasımlar Formation, embracing the Lower and Upper Carnian. The Kartoz Formation is only marginally represented by the lowermost 1.7 m of the log; this reflects a shallow palaeowater environment (massive limestone-bearing *in situ* reefs, megalodont bivalves, gastropods, sponges). The Kasımlar Formation, in turn, is represented by at least 33 m, bearing the Carbonate member (Julian 2), the Marlstone member and the Shale member (Tuvalian 1; Lukeneder *et al.* 2012, Lukeneder & Lukeneder 2014; Fig. 2). Based on its different facies description, the Carbonate member is subdivided into Carbonate member A (well-bedded

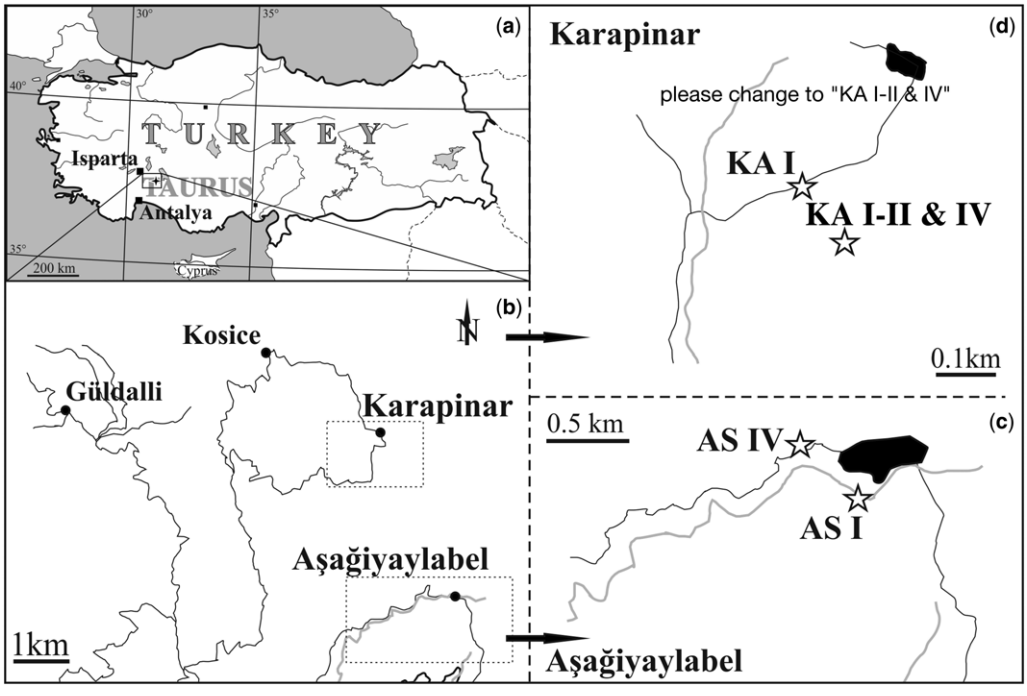

Fig. 1. (**a, b**) Geography of the sections at (**c**) Aşağiyaylabel (AS I, AS IV) and (**d**) Karapinar (KA I–II & IV) in the Taurus Mountains (Anatolia, Turkey).

dark-grey limestones yielding *Kasimlarceltites krystyni* in masses), B (Cipit-like boulders = mixed carbonate blocks embedded within reworked material) and C (well-bedded dark-grey limestones bearing millimetre-thick spherical bioturbations). The overlying Marlstone member consists of ochre, marly limestones which fade at the top into tectonically laminated shales (Fig. 2). The whole 33 m of the Kasımlar log represents a maximum time interval of 1.89–5.5 Ma (Ogg 2012; Lukeneder & Lukeneder 2014). This big difference in absolute values reflects an extreme divergence of two different chronostratigraphic models used for the absolute durations of the Upper Triassic (Ogg 2012). Whilst one model suggests a longer duration of Tuvalian time, the other suggests a longer Rhaetian duration. The deposits of the section AS I show an inclination of *c.* 50° towards NE. The whole facies description of AS I (Lukeneder *et al.* 2012) is summarized in Table 1.

Aşağiyaylabel IV (AS IV). The sequence starts with 14.5 m of massive shallow-water limestone (equivalent to the Kartoz Formation at AS I), yielding coral debris, sponges and bivalves (articulated and disarticulated). This is followed by 4 m of dark-grey, bedded ammonoid limestones (equivalent to Unit A at AS I; Fig. 2), bearing abundant *K. krystyni.* Event beds, which bear masses of *K. krystyni,* alternate with beds exhibiting only rare specimens of *K. krystyni*. The bedded limestones are overlain by 5.2 m of reworked material (equivalent to Unit B of AS I with Cipit boulders) and are sealed by a calcite layer; this may indicate tectonic faulting of undefined dimension. This is tectonically overlain by 3 m of carbonate reef-limestones yielding crinoid debris, and is topped by 0.5 m of coral limestone bearing coral debris, sponges and articulated bivalves (Figs 2–4, Table 1).

Karapinar I (KA I). The section Karapinar I (KA I) has one of the shortest but most characteristic sequences, represented by only 0.5 m of shallow-water limestones followed by a 5.5 m-thick bedded *Kasimlarceltites*-limestone sequence (Fig. 2). The shallow-water limestone and deeper-water limestone layers are tectonically overturned. The lithological transition from the shallow-water carbonates of the Kartoz Formation into the ammonoid beds (*K. krystyni* mass occurrence) of the lowermost Kasımlar Formation is the main feature within the transitional part in all known sections (Figs 2–4, Table 1).

Karapinar II (KA II). KA II, situated close to KA I (100 m SE), yields a very similar sediment

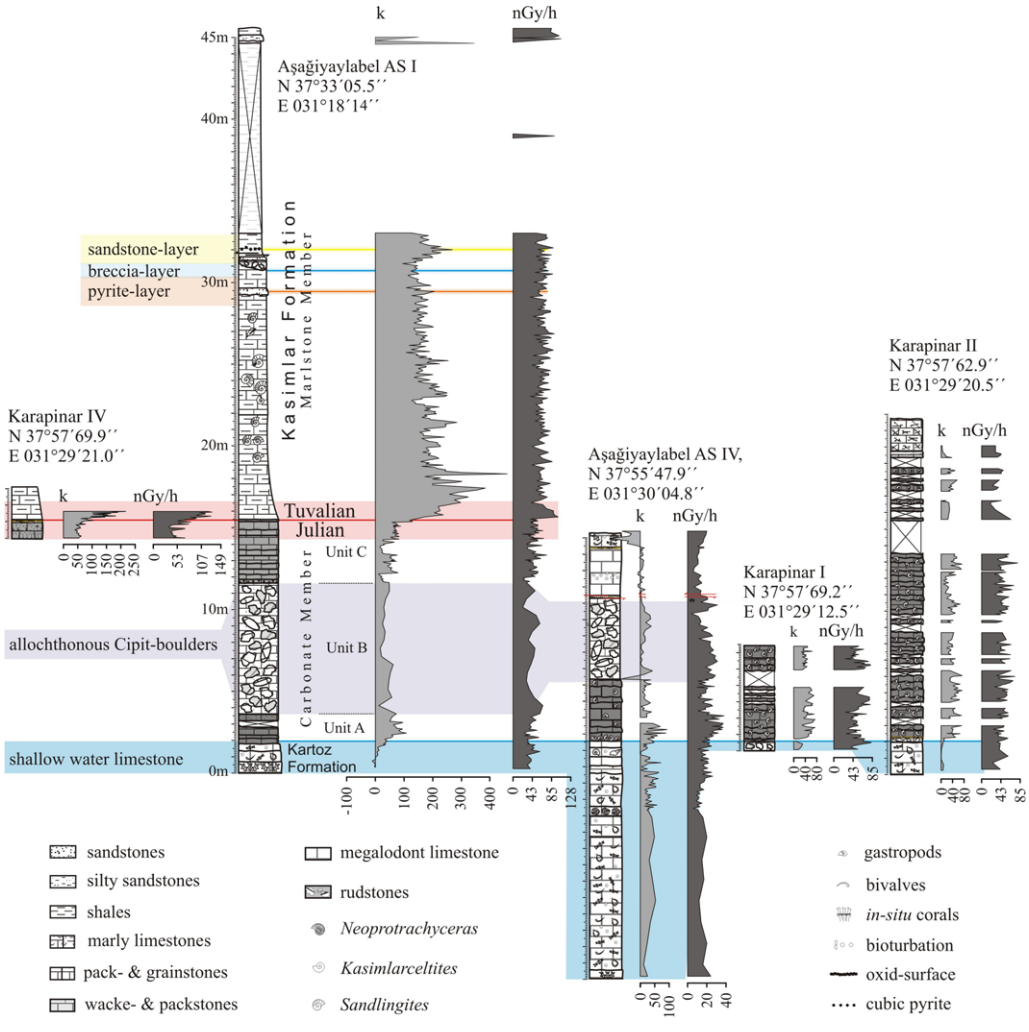

Fig. 2. Correlated logs of the sections AS I, AS IV and KA I–II & IV with corresponding magnetic susceptibility (MS: *k*) and radioactivity curves (nGy h^{-1}). *k*, value of volume MS in the natural state; nGy h^{-1}, dose rate.

sequence. The main difference is the extent of the ammonoid beds with their mass occurrence of *K. krystyni*. Shallow-water carbonates (which are equivalent to the Kartoz Formation of AS I) are replaced after 2 m by 17 m of black ammonoid beds (*K. krystyni* mass occurrence), equivalent to the *Kasimlarceltites* beds at the lowermost part of the Kasımlar Formation at AS I. This section seems to be more complete at the lower part of the Kasımlar Formation, causing an increased thickness of the ammonoid beds in comparison with AS I, AS IV and KA I. The top is formed by 2 m of dolomitized limestone. The shallow-water limestone and deeper-water limestone layers are characterized by a tectonically inverse stratification (Figs 2–4, Table 1).

Karapinar IV (KA IV). The section KA IV, about 100 m to the north of KA II, represents the shortest, but probably the most important, sequence. It comprises the Lower Carnian (Julian) to Upper Carnian (Tuvalian) facies change with its typical boundary strata, ranging from marly limestones into marlstones. The section is equivalent to the corresponding part at the main section at Aşağiyaylabel (AS I), where the Carbonate member (Unit C, Julian 2) is followed by the Tuvalian Marlstone member above. The abrupt change from the 1 m-thick dark-grey carbonate sequence to ochre marlstones is obvious and is a clear marker level in that area (Fig. 2). Two metres of marlstones are directly visible, but an unknown thickness of marlstones


(a)
AS I
(b)
AS IV
(c)
KA I
(d)
KA II
(e)
AS I
(f)
AS IV
(g)
Kasimlar Formation
Kartoz Formation
AS I

is covered by erosional sediments (Figs 2 & 4, Table 1).

Methodology

Magnetic Susceptibility (MS) was measured directly in the field with a hand-held, highly sensitive (1×10^{-7}, measured in SI units; results are indicated throughout as 'value $\times 10^{-6}$ SI'), low-level SM-30 MS meter (GF Instruments) bearing a 50-mm pick-up coil. Bed-by-bed measurements were conducted at distinct beds (e.g. Carbonate member Units A and C). This approach was replaced by a measuring interval of between 5 and 50 cm where distinct beds were missing (e.g. Carbonate member Unit C and Marlstone member);186 measurements of MS were performed in sediments of the Kartoz and Kasımlar Formations at AS I; 171 at AS IV; 85 at KA I; 156 at KA II; and 38 at KA IV. Each single bed was measured at least three times and the average calculated. To prevent measurement errors due to the sensitivity of the hand-held instruments (uneven terrain and therefore variable distance between coil and rock surface), a fresh smooth surface was prepared for each single point measured.

The radiometry was also conducted directly in the field using a hand-held scintillation gamma radiometer (GF Instruments), bearing a 51×51 mm (6 in^3) NaI (Tl) detector. Measurements were taken with an acquisition time of 1 s and a sampling interval between 5 and 50 cm through the whole log. We applied this method as an additional correlation tool and therefore concentrated on the dose rate (nGy h^{-1}) without testing the spectral results (K, U or Th): such detailed information is not supported by the instruments used. The resulting values were transposed to curves (using Microsoft Excel) and correlated with the log (Fig. 2). Furthermore we tested the correlation between the MS and radiometry signal for each sequence. The measurements were carried out during several field trips from October 2010 to October 2012 by the Natural History Museum Vienna (NHMV). In contrast to most studies, which focus on cyclostratigraphic results and therefore use highly sensitive laboratory measurements along with high-resolution measuring intervals, this study focused only on the MS and radiometry trends in order to correlate different logs of a regional area. Accordingly, data were measured directly in the field at the main locality (AS I) as well as at additional surrounding sites (AS IV, KA I–II & IV) with a maximum measuring interval of 50 cm. Samples did not receive any special preceding preparation; 152 radiometry measurements were performed in sediments of the Kartoz and Kasımlar Formations at AS I; 155 at AS IV; 81 at KA I; 132 at KA II; and 33 at KA IV. Data were subsequently compared with facies analyses and biostratigraphic data of AS I (Lukeneder *et al.* 2012; Lukeneder & Lukeneder 2014) as well as with sections from nearby localities (AS IV, KA I–II & IV).

Results of MS & radiometry measurements

General trends in MS in comparison with the $CaCO_3$ content

A general increase in the MS values from shallow-water platform limestones over bedded limestones up to the marlstones is evident within all five sections and logs at Aşağiyaylabel and Karapinar (Fig. 2, Table 2). The most drastic difference can be recognized within both logs from AS I and KA IV in the median values between the bedded limestones (58×10^{-6} SI and 56×10^{-6} SI for AS I and KA IV, respectively) and the marlstones (171×10^{-6} SI and 142×10^{-6} SI for AS I and KA IV, respectively). This corresponds to the Julian/Tuvalian boundary (i.e. Lower /Upper Carnian boundary). At this boundary the $CaCO_3$ content at AS I decreases from about 70% at the Julian Carbonate member to 60% and lower at the Tuvalian Marlstone member. The same trend is present at KA IV: the $CaCO_3$ content decreases from $>$ 55% at the Julian Carbonate member to $<$30% from the Tuvalian Marlstone member onward. Although their MS range overlaps (11 to 105×10^{-6} SI v. 62 to 458×10^{-6} SI), a general increasing trend is clearly recognizable (Table 2). The trends and positive shift in the MS curves can be precisely detected within the logs of AS and KA (Fig. 2).

Shallow-water carbonates: Kartoz Formation. The shallow-water carbonates of the Kartoz Formation are generally related to diamagnetic substances (Dearing 1999) and therefore show, as expected, negative MS values. The shallow-water platform carbonates, which partly bear *in situ* corals (Figs 2

Fig. 3. Detailed views of the shallow-water carbonates from the Kartoz Formation of the sections of Aşağiyaylabel (AS I, AS IV) and Karapinar (KA I, KA II). Platform carbonates with *in situ* corals from sections (**a**) AS I and (**b**) AS IV. Shallow-water reef-debris limestones from (**c**) KA I, (**d**) KA II, (**e**) AS I and (**f**) AS IV. (**g**) Transition from shallow-water carbonates from the Kartoz Formation into well-bedded *Kasimlarceltites* beds at the base of the Kasımlar Formation (Carbonate member) at AS I.

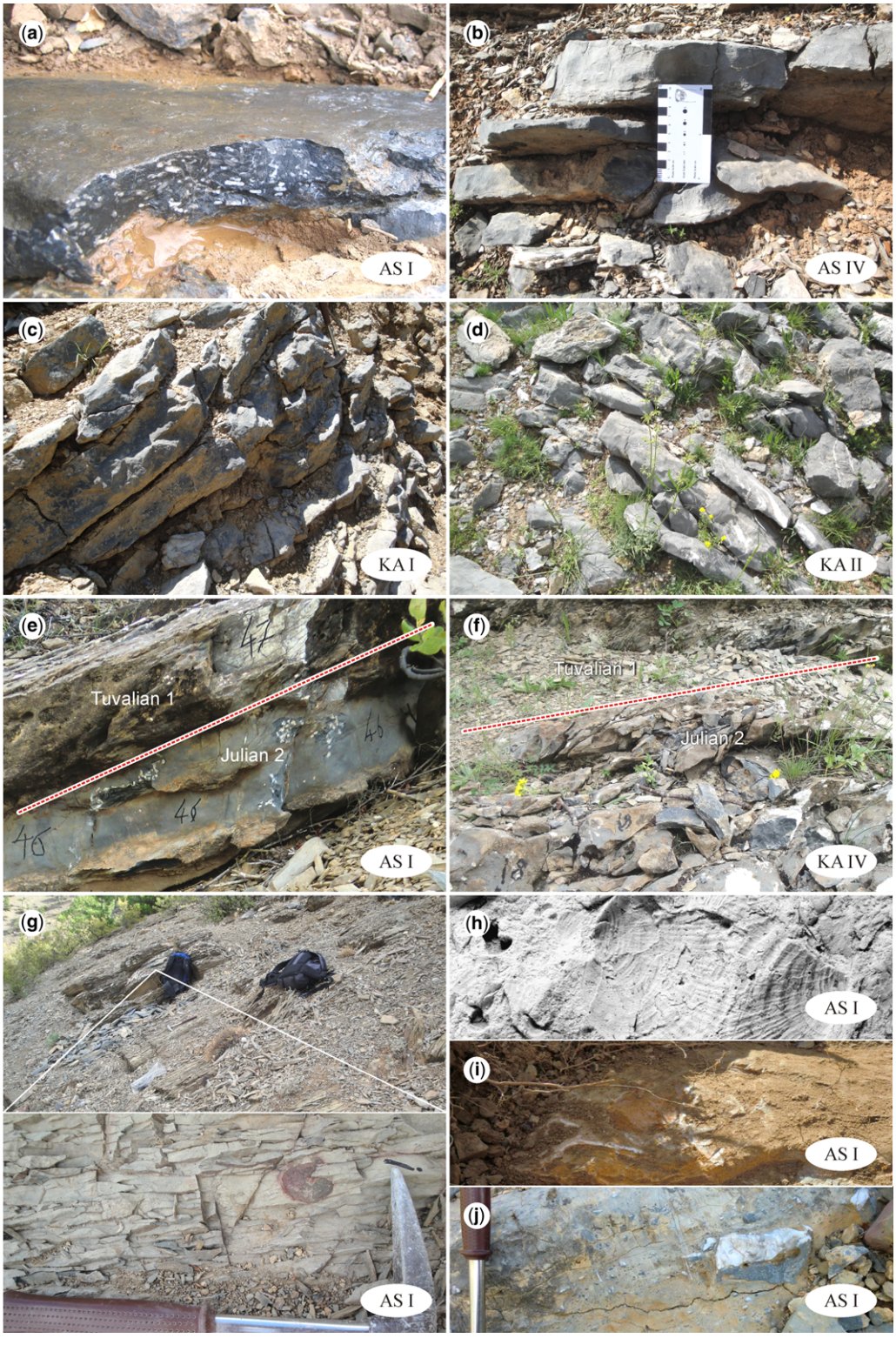
(a)
AS I
(b)
AS IV
(c)
KA I
(d)
KA II
(e)
Tuvalian 1
Julian 2
AS I
(f)
Tuvalian 1
Julian 2
KA IV
(g)
AS I
(h)
AS I
(i)
AS I
(j)
AS I

Table 2. *Magnetic susceptibility values (k) of the sections from Aşağiyaylabel (AS I, AS IV) and Karapinar (KA I, KA II, KA IV), measured in SI units: values need to be multiplied by 10^{-6}*

Facies		AS I	AS IV	KA I	KA II	KA IV	AS - KA
Shallow-water limestones with *in situ* corals	Range	−11–2	11–49	–	–	–	−11–49
	Median	−5	35	–	–	–	
Shallow-water limestones	Range	−3–36	−1–71	6–31	0–11	–	−3–71
	Median	9	26	22	7	–	
Cipit-like boulders	Range	12–62	1–42	–	–	–	1–62
	Median	35	12	–	–	–	
Well-bedded limestones with *Kasimlarceltites*	Range	33–108	3–93	16–74	4–72	–	3–108
	Median	61	24	43	36	–	
Well-bedded limestones with spherical percipitations	Range	11–96	–	–	–	40–105	11–105
	Median	58	–	–	–	56	
Calcareous marls to marlstones	Range	94–458	–	–	–	62–217	62–458
	Median	171	–	–	–	142	
Top Julian 2	–	96	–	–	–	84	
Bottom Tuvalian 1	–	119	–	–	–	83	
Sandstone layer	–	136	–	–	–	–	
Breccia layer	–	120	–	–	–	–	
Pyrite layer	–	200	–	–	–	–	

& 3a–d), show very similar MS values as well as similar $CaCO_3$ contents (92.9–95.8%). Hence a differentiation based on MS signals or $CaCO_3$ content is not possible in these shallow-water carbonates from the Kartoz Formation. Nevertheless, the lowest MS values are clearly much lower within carbonate deposits having *in situ* corals (minimum -11×10^{-6} SI) than within deposits of shallow-water limestones without *in situ* corals (minimum -3×10^{-6} SI). Furthermore a generally higher trend of MS values is observable at the shallow-water limestones without *in situ* corals (-11 to 49×10^{-6} SI v. -3 to 71×10^{-6} SI).

Kasimlarceltites limestones: Kasımlar Formation (Carbonate member Unit A). Well-bedded *Kasimlarceltites* limestones occur in almost every log, except for KA IV due to its different stratigraphic position (Figs 2 & 4a–d). The MS values of these black ammonoid beds range between 3 and 93×10^{-6} SI at AS IV, between 33 and 108×10^{-6} SI at AS I, between 16 and 74×10^{-6} SI at KA I, and between 4 and 72×10^{-6} SI at KA II. Their values are generally slightly higher than those of the shallow-water limestone deposits (-11 to 71×10^{-6} SI; Table 2). While their median values are not always higher than the median values of the shallow-water limestones, their maxima are higher by far within all sections (108×10^{-6} v. 36×10^{-6} SI at AS I; 93×10^{-6} v. 71×10^{-6} SI at AS IV; 74×10^{-6} v. 31×10^{-6} SI at KA I; 72×10^{-6} v. 11×10^{-6} SI at KA II; Fig. 2, Table 2). The carbonate content in all sections (average 90.6%) is significantly lower than in the shallow-water carbonates (94.1%). This decrease corresponds well to the increase in terrigenous material.

Cipit-like boulders: Kasımlar Formation (Carbonate member Unit B). An interval with Cipit-like boulders (these being metre- to tens-of-metre-sized isolated blocks embedded in different kinds of sediments; see Richthofen (1860) and Lukeneder *et al.* (2012)) was detected in the Carbonate member (Unit B, Kasımlar Formation) within both sections of Aşağiyaylabel (AS I and AS IV; Fig. 2). Cipit-like boulders represent a mixture of allochthonous material from different source areas (e.g. shallow-water environments and deeper deposits), making it impossible to distinguish such sediments

Fig. 4. Detailed views of the deeper-water carbonates (Units A, B, C) and the calcareous marls to marlstones of the Marlstone member from the Kasımlar Formation of the Aşağiyaylabel (AS I, AS IV) and Karapinar (KA I–II & IV) sections. Well-bedded *Kasimlarceltites* beds at the base of the Kasımlar Formation (Carbonate member, Unit A) at the sections (**a**) AS I, (**b**) AS IV, (**c**) KA I and (**d**) KA II. Julian/Tuvalian boundary (Lower/Upper Carnian boundary) at the carbonate/marl transitional intervals at the sections (**e**) AS I and (**f**) KA IV within the Kasımlar Formations at the top of Unit C, below the Marlstone member. (**g**) Characteristic marls of the Marlstone member (AS I) within the Kasımlar Formation bearing the abundant Tuvalian ammonoid *Paratropites* cf. *hoetzendorfii*. (**h**) Layer with accumulation of the bivalve *Halobia* and pyrite cubes within the Marlstone member from AS I. (**i**) Sandstone layer of the Marlstone member, AS I. (**j**) Breccia layer with shallow-water components within the Marlstone member, AS I.

from the sediments of the shallow-water limestone sequence (Kartoz Formation) using MS data. Although the MS values show a broad overlap with those of the bedded limestones, the maxima and medians are much lower (maximum 62×10^{-6} SI at AS I; median 35×10^{-6} SI at AS I resp. 12×10^{-6} SI at AS IV) than in the well-bedded limestones (maximum 108×10^{-6} SI at AS I; median 61×10^{-6} SI at AS I resp. 24×10^{-6} SI at AS IV). Additionally, Cipit beds appear with considerably lower values than the marly limestones (equivalent to the Marlstone member; 1 to 62×10^{-6} SI v. 62 to 458×10^{-6} SI). Nevertheless, the average $CaCO_3$ content at the Cipit-like boulders at AS I (87.9%) is slightly lower than at the shallow-water limestones (average 94.1%) and the *Kasimlarceltites* beds (average 90.6%; Fig. 2, Table 2).

Well-bedded limestones with spherical precipitations: Kasımlar Formation (Carbonate member Unit C). Dark-grey to black, well-bedded limestones of the Carbonate member Unit C comprising spherical millimetre- to centimetre-sized precipitations (without *Kasimlarceltites*) occur only at the sequences AS I and KA IV (Fig. 4e, f). Unit C is located directly below the Julian/Tuvalian boundary. The MS values, with a median value of 58×10^{-6} SI (at AS I) resp. of 56×10^{-6} SI (at KA IV), are almost identical to those of the bedded limestones bearing *Kasimlarceltites* in Unit A of AS I (median $= 61 \times 10^{-6}$ SI). Nevertheless, the average $CaCO_3$ contents are, in contrast to those at the *Kasimlarceltites* limestones (Unit A), significantly lower: 80.5% at AS I and 86.4% at KA IV (v. 94.1% at AS I; Fig. 2, Table 2).

Marly limestones: Kasımlar Formation (Marlstone member). As described above, the MS values of the calcareous marls and marlstones (Marlstone member at AS I and KA IV; Figs 2 & 4g, Table 2) are significantly higher than those from the carbonates of the Kartoz Formation and the underlying Carbonate member of the Kasımlar Formation. The MS data show higher maxima (458×10^{-6} SI at ASI resp. 217×10^{-6} SI at KA IV), and also higher median values (171×10^{-6} SI at AS I resp. 142×10^{-6} SI at KA IV). This increase starts exactly at the Julian/Tuvalian boundary (Fig. 2, Table 2). A drop in carbonate content (average 26.77% at KA IV and 30.6% at AS I) goes hand in hand with this major positive shift in MS values.

Sandstone layer, breccia layer, pyrite layer: Kasımlar Formation (Marlstone member). Due to the higher content of paramagnetic minerals such as pyrite (FeS_2) within the pyrite layer or glauconite ($(K, NA)(Fe^{3+}, Al, Mg)_2(Si, Al)_4O_{10})(OH)_2$) within the sandstone layer, described by Lukeneder *et al.* (2012), some peaks are probably related to lithologically identified pyrite concentrations (200×10^{-6} SI) or sandstone layers (136×10^{-6} SI; Figs 2 & 4h–i, Table 2). The distinct sandstone layer, breccia layer and pyrite layer are detected exclusively within the Marlstone member at the AS I section (Fig. 2). We therefore assume that the range of peaks in the MS curve at the Marlstone member can be assigned to such characteristic event beds or layers and are indicative for marginal breccias, glauconite or pyrite layers, which are hardly detectable without geophysical measurements (Figs 2 & 4h–j).

MS measurements at Aşağiyaylabel and Karapinar generally reflect the influence of a terrigenous input. Higher susceptibility values argue for an increased entry of terrigenous material, additionally reflected by a decrease in the carbonate content.

The radiometry measurements

The radiometry variation of a studied section reflects the presence of detrital clays, feldspars, heavy minerals and other minerals arriving by riverine, aeolian or other inputs (Serra *et al.* 1980; Serra 1984; Rider 1990). Higher radiometry may reflect higher clay content. Measurements of radiometry response (nGy h^{-1}) are a powerful tool for interpreting lithological changes within an outcrop (Lukeneder *et al.* 2010).

The radiometry values confirm the increasing trend and positive shift already described by the MS values at the Julian/Tuvalian boundary at AS I and KA IV (Fig. 2, Table 3). Shallow-water limestones (Kartoz Formation) and well-bedded ammonoid limestones (Kasımlar Formation, Carbonate member, Unit A) are not well distinguishable by the radiometry data (Fig. 2, Table 3). A significant increase is recognizable again at the Lower/Upper Carnian boundary beds (Julian 2/Tuvalian 1) at AS I and KA IV. The positive shift in radiometry values marks the change from well-bedded carbonates of the Carbonate member (Unit C) to the calcareous marls and marlstones of the Marlstone member, both within the Kasımlar Formation (Fig. 2).

Kartoz Formation and Kasımlar Formation with Carbonate member (Units A–C). The whole sequences of the Kartoz Formation (shallow-water limestones partly with *in situ* corals) and the Carbonate member of the Kasımlar Formation (well-bedded ammonoid limestones Unit A, Cipit interval Unit B, well-bedded limestones Unit C) are hardly distinguishable from each other by means of their radiometry values (Figs 2 & 3g, Table 3). Their general radiometry ranges are very similar, except

Table 3. *Radiometry values (nGy h^{-1}) of the section from Aşağiyaylabel (AS I, AS IV) and Karapinar (KA I–II & IV)*

Facies		AS I	AS IV	KA I	KA II	KA IV	AS - KA
Shallow-water limestones with *in situ* corals	Range	32.03–40.57	25.62–51.24				25.62–51.24
	Median	38.43	34.16				
Shallow-water limestones	Range	29.89–59.78	12.81–55.51	38.43–83.27	23.49–57.65		12.81–83.27
	Median	40.57	34.16	56.58	40.57		
Cipit-like boulders	Range	23.49–66.19	8.54–66.19				8.54–66.19
	Median	42.7	46.97				
Well-bedded limestones with *Kasimlarceltites*	Range	25.62–57.65	21.35–81.13	25.62–81.13	17.08–79		17.08–81.13
	Median	33.09	46.97	51.24	44.84		
Well-bedded limestones with spherical percipitations	Range	21.35–74.73				34.16–83.27	21.35–83.27
	Median	44.84				51.24	
Calcareous marls to marlstones	Range	38.43–100.35				83.27–130.24	38.43–130.24
	Median	66.19				106.75	
Top Julian 2		55.51				70.46	
Bottom Tuvalian 1		44.84				91.81	
Sandstone layer		55.51					
Breccia layer		79					
Pyrite layer		68.32					

for the maximum values of the layers comprising *in situ* corals at AS I (40.57 nGy h^{-1}) and AS IV (51.24 nGy h^{-1}). These radiometry values are slightly lower than the maxima of the shallow-water limestones (59.78 nGy h^{-1} at AS I, 55.51 nGy h^{-1} at AS IV, 83.27 nGy h^{-1} at KA I, and 57,65 nGy h^{-1} at KA II). They are also lower than the maximum at the interval (Unit B) with Cipit-like boulders (66.19 nGy h^{-1} at AS I and AS IV) and the maxima at the bedded limestones with spherical precipitation (Unit C) (74.73 nGy h^{-1} at AS I and 83.27 nGy h^{-1} at KA IV).

Calcareous marls and marlstones: Kasımlar Formation (Marlstone member). The radiometry values of the calcareous marls and marlstones are generally higher than in all underlying sediment deposits (e.g. Kartoz Formation and Carbonate member of the Kasımlar Formation; Fig. 4g, Table 3). The positive shift in radiometry values is most distinct at section KA IV (Fig. 2), where the values of the Carbonate member range between 34.16 and 83.27 nGy h^{-1} (median 51.24 nGy h^{-1}). The values of the calcareous marls and marlstones lie between 83.27 and 130.24 nGy h^{-1} (median 106.75 nGy h^{-1}). Although the difference is not as significant at section AS I, and ranges overlap (21.35–74.73 nGy h^{-1} in limestones of Unit C compared to 38.43–100.35 nGy h^{-1} in calcareous marls and marlstones), an increase of the radiometry values is clearly recognizable. This is especially evident when comparing the median radiometry values, which is lower (44.84 nGy h^{-1}) in the carbonate parts than in the more marly parts of section AS I (66.19 nGy h^{-1}).

Sandstone layer, breccia layer, pyrite layer: Kasımlar Formation (Marlstone member). The MS peaks from the Marlstone member within the AS I section, already mentioned within the MS-result chapter above, are just as recognizable within the radiometry values. These are related to thin event layers, for example, sandstone layers (55.51 nGy h^{-1} at AS I; Fig. 4i), breccia layers (79 nGy h^{-1} at AS I; with shallow-water components; Fig. 4j, Table 3) or pyrite layers (68.32 nGy h^{-1}; with pyrite and goethite). These peaks, however, are less significant than the MS values.

Radiometry and MS data correlation: time-series analysis

For comparing the MS and radiometry curves (Fig. 5), we only used data from beds at which both measurements were available. The time alignment of both signals (MS and radiometry) was tested by using cross correlation of two time series with the correlation coefficient r (Davis 1986; Hammer & Harper 2006). Cross correlation is used for optimal alignment of two series (Hammer *et al.* 2008). To do this, one time series is kept in a fixed position, whilst the second time series is slid past, and for each position, the correlation coefficient (r) computed (Fig. 5, black line). The correlation coefficient (r; black line) is then plotted as a function of alignment position (Hammer & Harper 2006). The horizontal axis (x) represents the displacement of the radiometry data with respect to the MS data, whilst the vertical axis (y) shows the correlation of both time series for a given displacement. Therefore, the position with the highest correlation coefficient indicates optimal adjustment. Significance is shown by plotting the p-values (Fig. 5; grey line). Correlation coefficients (r; black line), which show higher values than the corresponding p-values (grey line), indicate a significant correlation. For a more detailed description of time-series analyses see Hammer & Harper (2006) and Hammer *et al.* (2008).

The results (Fig. 5) clearly reveal that both curves of the section AS I and KA IV correlate significantly. A significant peak positive correlation occurs at AS I in the region of two samples delay of the MS signal with respect to the radiometry signal (see Fig. 5). This is in contrast to the sections AS IV and KA I–II, where no significant correlation between the two signals was observed. Moreover, certain sequences of AS I do not show positive correlations between the MS and radiometry signals. Examples are the *Kasimlarceltites* beds, or from the top of the Marlstone member onward, where the homogeneous marlstone beds start to alternate with sandstone, breccia and pyrite layers; this might affect the MS signal more significantly than the radiometry signal.

MS and radiometry data used for the correlation of time-equivalent sequences

The investigated MS and radiometry data from the area around Aşağiyaylabel and Karapinar are the first to have been measured from Lower to Upper Carnian carbonate sequences. At section AS I, the Julian/Tuvalian boundary could be fixed by ammonoid biostratigraphy (Lukeneder & Lukeneder 2014) and facies analyses (Lukeneder *et al.* 2012).

In the present study, the characteristic lithological change exactly at the Julian/Tuvalian boundary from well-bedded limestones (Unit C) into calcareous marls and marlstones (i.e. Marlstone member at AS I and KA IV) is demonstrated by a distinct MS increase from 58×10^{-6} SI at AS I resp. 56×10^{-6} SI at KA IV to 171×10^{-6} SI at AS I resp. 142×10^{-6} SI at KA IV. A similar increase in radiometry values is observed from 44.84 nGy h^{-1} at AS I resp. 51.24 nGy h^{-1} at KA

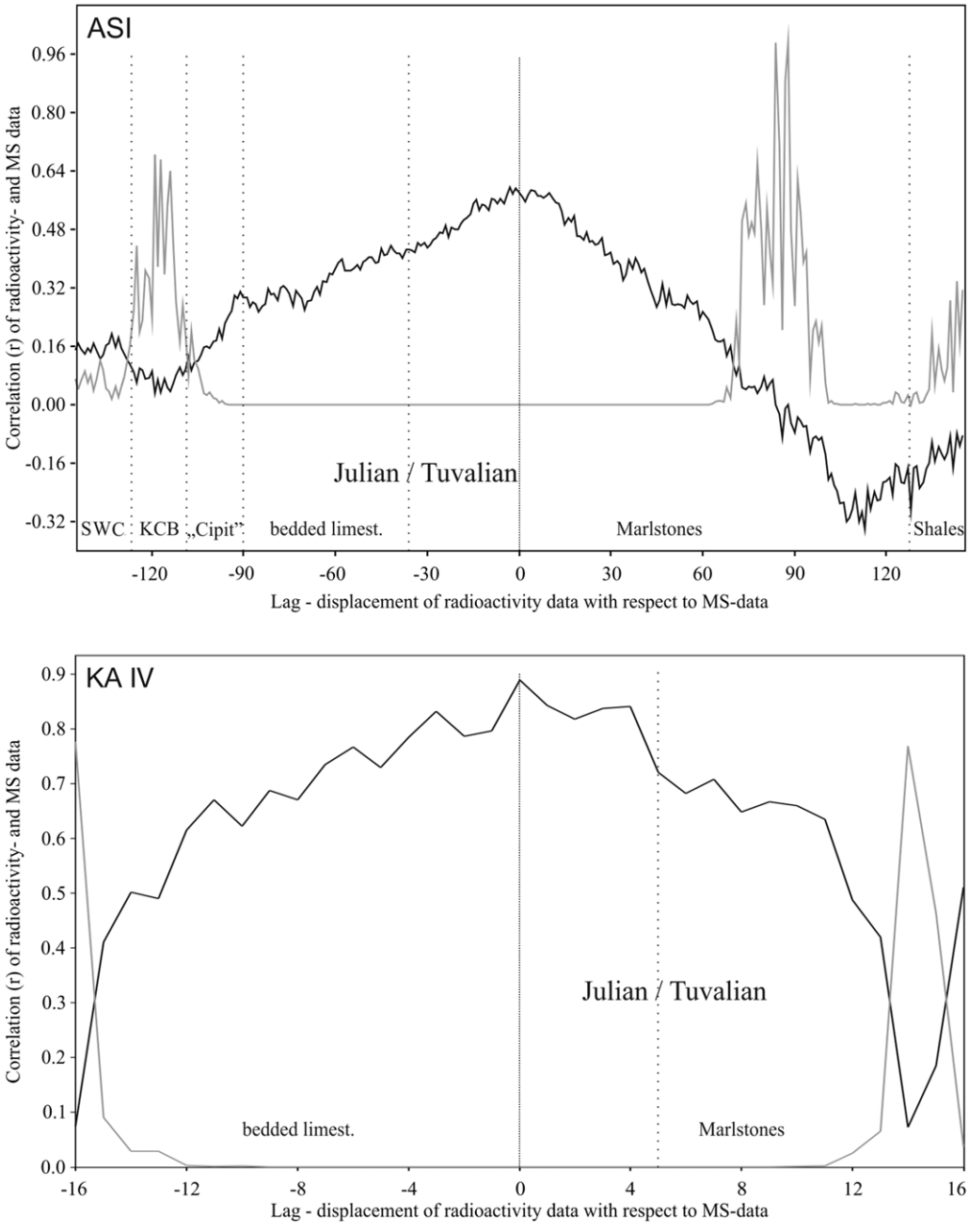

Fig. 5. Cross correlation of magnetic susceptibility values v. radiometry values from the sequence AS I. Black line represents the correlation coefficient r, whilst the grey line represents the significance in p-values. SWC, Shallow water carbonates; KCB, *Kasimlarceltites* beds.

IV to 66.19 nGy h^{-1} at AS I resp. 106.75 nGy h^{-1} at KA IV (Figs 2 & 5, Tables 2 & 3). MS and radiometry signals from section AS I were then compared with those from additional sections at Aşağiyaylabel (AS IV) and Karapinar (KA I–II & IV). The intention was to localize a specific part of the sequence at these sections, namely that part which possibly also bears an equivalent of the Julian/Tuvalian

boundary. The opportunity to detect such important and characteristic biostratigraphic and lithological boundaries by geophysical measurements (e.g. MS and radiometry) is an additional, preliminary tool for correlation in the field. The measurements can be supported by subsequent measurements in laboratories (e.g. Kappabridge, Karl-Franzens-University, Graz), and ultimately proved by palaeontological and geological investigations. The MS studies, conducted here with hand-held instruments, can also easily be used to find characteristic features in sequences as sequence-boundaries, marked by lithological changes, even at sections where no macrofossil markers are detected in the field.

Sections AS IV and KA I–II lack this characteristic boundary. Section KA IV, however, which shows a similar lithological change from well-bedded calcareous limestones to marly limestones, shows an MS (up to 217×10^{-6} SI) and radiometry peak (up to 130.24 nGy h^{-1}) comparable to that found at the Julian/Tuvalian boundary at AS I (Fig. 5, Tables 2 & 3).

Radiometry and MS values studied by a time-series analysis show that in both cases (at sections AS I and KA IV) the curves are mostly significantly positively correlated (Fig. 5). Accordingly, the primary signal seems to be preserved (except for some parts discussed below).

Both signals show an abrupt increase at the Julian/Tuvalian boundary, which can be interpreted as an increased influx of detrital minerals into the system. The preceding demise of the carbonate platform and the decrease of the $CaCO_3$ content from the Julian to the Tuvalian sediments clearly reflect this siliciclastic entry. This entry probably affected fluviatile systems due to the more humid conditions, which are described in several studies dealing with the carbonate platform demise during Carnian time (Lukeneder *et al.* 2012). The possible trigger mechanisms for this extraordinary ecological incision are still under discussion and therefore the subject of a series of studies. One potential reason is an uplift of extended areas (e.g. the Fennoscandian High of the Cimmerian orogeny), which could have been a trigger for a monsoonal climate (Hornung & Brandner 2005; Preto *et al.* 2010). The resulting new landmasses could have been the source areas for the increased terrigenous input into the northwestern part of the Tethyan Sea. This influx might have led to the well-known carbonate platform demise within the Tethyan realm (Tollmann 1976; Aigner & Bachmann 1992; Hornung & Brandner 2005; Preto *et al.* 2010). Another plausible scenario is magmatic or volcanic activities (e.g. the volcanic series of the Wrangellia terrane or Eastern Mediterranean alkaline volcanics), which could have influenced oceanic circulation, resulting in global climate change (Hornung *et al.* 2007; Preto *et al.* 2010). Robinson (1973) and Parrish (1993) suggest that the wet climate during Carnian time might have been the peak of the monsoonal character that already existed during the transition from the Permian to the Triassic, and therefore can be traced back to the maximum aggregation of the landmasses at that time (Preto *et al.* 2010). The result was a hot and dry climate within the continent interior, alternating wet and dry seasons at the coast of eastern Laurasia and Gondwana (Parrish & Peterson 1988; Dubiel *et al.* 1991; Mutti & Weissert 1995), and a generally wet climate at higher latitudes (Robinson 1973; Preto *et al.* 2010). Furthermore, a sea-level drop, followed by submarine clathrate-destabilization and methane degassing (Hornung 2008), are also part of a large compendium of discussed scenarios along with dramatic sea-level rise (Arche & López-Gómez 2014), sediments representing anoxic events beneath siliciclastic sediments (Jerz 1966; Schuler 1968; Hagemeister 1988) and rapid variations in seawater chemistry.

Although the radiometry and MS signals generally correlate positively in both sequences (AS I and KA IV) at which the Julian/Tuvalian boundary was detected, certain intervals of AS I do not support this general correlation trend. This for instance is the case of the well-bedded limestones bearing *K. krystyni*, the top of the Marlstone member, as well as the whole Shale member of AS I, which might be caused, to some extent, by diagenetic overprint. The stylolitic structures (Table 1) observed within these beds would support this hypothesis. Nonetheless, the MS signals between these *Kasimlarceltites* beds of the different localities are rather similar (61×10^{-6} SI at AS I; 24×10^{-6} SI at AS IV; 43×10^{-6} SI at KA I; 36×10^{-6} SI at KA II), perhaps reflecting a similar diagenetic history of those beds.

These characteristic MS and radiometric peaks at the Julian/Tuvalian boundary can be used as additional stratigraphic correlation tools. Moreover, the other lithological parts (below and above) at AS I also show values similar to those of the surrounding sequences. Although the primary signals might be diagenetically overprinted (because the MS and radiometry signals do not show significant correlation), some comparisons between similar lithologies are possible and are therefore discussed:

Whilst at both AS I and KA II the carbonate platform sediments are represented by only 1.8-m-thick and 2.3-m-thick coral-limestones, respectively, the carbonate platform sediments at section AS IV is 14.5 m thick (Fig. 2). KA IV lacks the carbonate platform sediments, due to its higher stratigraphic position (Julian/Tuvalian boundary). The corresponding MS values of the shallow-water limestone deposits (AS I, AS IV, KA I, KA II; Fig. 2) are very low to negative (-11 to 71×10^{-6} SI), as already

estimated and expected for the diamagnetic mineral calcite (Algeo *et al.* 2007*a*). Ellwood & Ledbetter (1977) have already mentioned that MS values are inversely proportional to the $CaCO_3$ content of unconsolidated marine sediments. This fits well with the picture and data shown from Aşağiyaylabel and Karapinar: low MS values, from -11 to 71×10^{-6} SI, occur in shallow-water carbonates (Kartoz Formation), higher values, from 3 to 108×10^{-6} SI, are found in well-bedded limestones (Carbonate member, Kasımlar Formation), and much higher values, from 62 to 458×10^{-6} SI, occur in calcareous marls and marlstones (e.g. Tuvalian Marlstone member, Kasımlar Formation).

Algeo *et al.* (2007*b*) have described atypical positive instead of negative correlations between MS values and carbonate beds from the Permo-Triassic Guryul Ravine section in Kashmir (India). This Indian section should appear as diamagnetic due to its high calcite content (Algeo *et al.* 2007*b*). Algeo *et al.* (2007*b*) explained this positive correlation with the theory that the carbonate fossil concentrations might be produced by winnowing, yielding incorporated paramagnetic heavy minerals which potentially cause the higher MS signal (Ellwood *et al.* 2000; Algeo *et al.* 2007*b*). The Indian example shows that MS values should always be used cautiously and interpreted solely in combination with facies analyses and different available proxies.

In contrast to the shallow-water carbonates with almost pure limestones, the overlying dark-grey, well-bedded limestones, which bear masses of *K. krystyni*, occur in nearly every section (Unit A at AS I, AS IV, KA I, KA II). Nonetheless, they differ in thickness: whereas at the main section (AS I) the shell beds are condensed and reduced to only 1 m, AS IV bears *c.* 4 m, KA I >4 m, and KA II *c.* 17 m. The MS values increase slightly with the onset of the *Kasimlarceltites* limestones, observable at all sections (AS I, AS IV, KA I, KA II) where such beds are detectable. This positive trend indicates the beginning of the demise due to the onset of the siliciclastic runoff. The allochthonous intervals with Cipit-like boulders in Unit B (Carbonate member, Kasımlar Formation) of the sections AS I and AS IV reflect lower MS values due to the shallower carbonate source areas (shallow platform).

The sudden demise of the carbonate platform at the main section AS I, represented by the shift from shallow-water limestones bearing *in situ* corals over shallow-water limestones to bedded limestones and calcareous marls and marlstones, is interpreted as being caused by an increased input of siliciclastic material from the hinterland, triggered by more humid conditions (Lukeneder *et al.* 2012). Due to similar deposits and the similar MS and radiometry trend of the correlated sequences (AS IV, KA I, KA II), the local deepening can be interpreted at least as a regional event that affected a recent area of at least 2.8 km diameter (Aşağiyaylabel to Karapinar).

As mentioned above, we used the MS and radiometry results with caution and interpreted them solely as a trend. This is because we measured them directly in the field without highly sensitive laboratory methods and without special preceding sample preparation. Nonetheless, specific trends and shifts in MS and radiometry values can be detected and are used in combination with other analyses (e.g. geochemistry, facies changes, biostratigraphy). This interdisciplinary approach was particularly successful with regard to the characteristic peaks at the Julian/Tuvalian boundary. Additional distinct peaks along the MS curve, detected within the Marlstone member (AS I), are significant and are well correlated to a single sandstone layer, as well as to a distinct pyrite layer. Although pyrite is a paramagnetic mineral and generally shows low positive susceptibility values, the above-mentioned pyrite layer appears with values of 200×10^{-6} SI. Therefore it is remarkable that such high susceptibility values can be associated with pyrite. Nonetheless, other minerals exhibit stronger paramagnetism than pyrite, such as biotites or certain iron silicates (Dunlop & Özdemir 1997). Moreover, this could hint at partly oxidized pyrite which is probably associated with some magnetite or maghemite, and might be caused by the formation of magnetite or goethite (Lazaroff 1997). Such high values therefore indicate the occurrence of a range of distinct and thin event layers as sandstone and pyrite layers (e.g. AS I, top of marlstone beds). These are lithologically hardly observable in the field but easily detectable by geophysical measurements (e.g. hand-held MS). This shows that MS data and radiometry measurements, along with a trendline and shift interpretation undertaken by comparing and proving already-analysed lithological parameters, are valid methods for a better understanding of stratigraphic and palaeontological datasets. Geophysical measurements, although performed in the field by hand-held instruments, can hint at characteristic parts or layers within sections that are different and yet can be correlated. They can serve as a preliminary tool for subsequent stratigraphic investigations. MS and radiometry data are thus significant proxies for the amount of siliciclastic input, which in turn might reflect some climatic conditions.

Conclusions

This study presents the first magnetic susceptibility (MS) and radiometry signature of Lower to

Upper Carnian sediments. The results from the MS and radiometry logs of the sections are therefore only comparable among themselves (AS I, AS IV and KA I–II & IV). The investigated section comprises the important Julian/Tuvalian substage boundary (=Lower/Upper Carnian boundary) within the Kasımlar Formation, recently detected at Aşağiyaylabel (Taurus Mountains, Turkey). The data are interpreted solely as a trend. Nonetheless, an indicative shift of the MS values (11 to 105 $\times$ 10^{-6} SI up to 62 to 458 $\times$ 10^{-6} SI) and an increase of the radiometry values (21.35–83.27 nGy h^{-1} up to 38.43–130.24 nGy h^{-1}) perfectly reflect the Julian/Tuvalian (Lower/Upper Carnian) boundary at the sections AS I and KA IV (Fig. 2, Tables 2 & 3). The Julian/Tuvalian boundary is of special interest due to its key position at the beginning of the Carnian Crisis within this area. The boundary is characterized by the change from a carbonate system into a marl-dominated system, triggered by severe climate change during Lower to Upper Carnian time. The Julian/Tuvalian boundary was already indicated by biostratigraphic investigations and facies analyses (Lukeneder *et al.* 2012; Lukeneder & Lukeneder 2014), strengthened herein by the MS and radiometry data from several sections. A second, smaller positive shift in MS and radiometry values is observed at Aşağiyaylabel and Karapinar at the transition from shallow-water carbonates of the Kartoz Formation to deeper-water carbonates from the base of the Kasımlar Formation at its ammonoid beds (AS I, AS IV, KA I, KA II). The latter shift is typical for a transition from pure carbonates to more marly limestones. This seems to have been caused by an increasing amount of siliciclastic material, which accumulated within the northwestern Tethyan shelves and basins due to the onset of increased river runoff, probably triggered by humid conditions. The situation is prolonged and more pronounced at the Julian/Tuvalian boundary when the Carnian Crisis (=Carnian Pluvial Event) started at the western end of the Cimmerian Terranes, as postulated by numerous studies (e.g. Tollmann 1976; Simms & Ruffell 1989; Aigner & Bachmann 1992; Hornung & Brandner 2005; Kozur & Bachmann 2010; Lukeneder *et al.* 2012). This more humid climate phase, with increased terrigenous and siliciclastic input, occurs somewhat later in the Taurus Mountains than in other sections of various European areas (Lukeneder *et al.* 2012).

This study shows that MS and radiometry data, used with caution and in combination with facies analyses and biostratigraphic investigations, constitute a robust tool to detect lithological changes by quantitative trendlines. Additionally, very thin and distinct layers in the otherwise-uniform marls can be detected by the MS measurements. Such event beds are formed by brief but high input of siliciclastic material such as breccia, pyrite accumulation and sandstones. This trendline method, performed by hand-held MS and radiometry instruments, is straightforward, fast, inexpensive and non-destructive. We therefore suggest applying these geophysical methods as additional tools for comparing geological sections and logs. These geophysical approaches (using MS and radiometry devices) are more sensitive than biostratigraphic methods or facies analyses, making them useful tools to detect possible sequences for which more detailed biostratigraphic investigations should be conducted. They are also suitable for comparing logs at which proper biostratigraphic markers are not preserved. More exact data call for the additional use of laboratory equipment (e.g. Kappabridge, Karl-Franzens-University, Graz). This approach supports common facies analyses and palaeontological studies with quantitative data, enhancing the interpretation of past environmental conditions.

The study is part of project P 22109-B17, funded by the Austrian Science Fund (FWF). It was supported by the Turkish Geological Survey (MTA), which was responsible for approving digging permission within the area investigated. The authors appreciate the suggestions and comments of two anonymous reviewers which improved the quality of the manuscript. We thank the volume editor Simo Spassov (Royal Meteorological Institute of Belgium) for his positive advice. The authors thank Oleg Mandic (Natural History Museum Vienna) for useful comments concerning the MS and radiometry analyses, as well as Anton Englert and Franz Topka (both at the Natural History Museum Vienna) for sampling assistance and thin-section preparation.

References

Aigner, T. & Bachmann, G. H. 1992. Sequence stratigraphic framework of the German Triassic. *Sedimentary Geology*, **80**, 115–135.

Algeo, T. J., Ellwood, B., Nguyen, T. K. T., Rowe, H. & Maynard, J. B. 2007*a*. The Permian-Triassic boundary at Nhi Tao, Vietnam: evidence for recurrent influx of sulfidic watermasses to a shallow-marine carbonate platform. *Palaeogeography, Palaeoclimatology, Palaeoecology*, **252**, 304–327.

Algeo, T. J., Hannigan, R., Rowe, H., Brookfield, M., Baud, A., Krystyn, L. & Ellwood, B. B. 2007*b*. Sequencing events across the Permian-Triassic boundary, Guryul Ravine (Kashmir, India). *Palaeogeography, Palaeoclimatology, Palaeoecology*, **252**, 328–346.

Andrew, T. & Robertson, A. 2002. The Beyşehir-Hoyran-Hadim nappes: genesis and emplacement of Mesozoic marginal and oceanic units of the northern Neotethys in southern Turkey. *Journal of the Geological Society, London*, **159**, 529–543.

Arche, A. & López-Gómez, J. 2014. The Carnian Pluvial Event in Western Europe: new data from Iberia and

correlation with the Western Neotethys and Eastern North America – NW Africa regions. *Earth Science Reviews*, **128**, 196–231.

Babek, O., Kalvoda, J., Aretz, M., Cossey, P. J., De Vuyst, F.-X., Herbig, H.-G. & Sevastropulo, G. 2010. The correlation potential of magnetic susceptibility and outcrop gamma-ray logs at Tournaisian-Viséan boundary sections in Western Europe. *In*: Da Silva, A. C. & Boulvain, F. (eds) *Magnetic Susceptibility, Correlations and Palaeozoic Environments*. Geologica Belgica, Brussels, **13**, 291–308.

Crick, R. E., Ellwood, B. B., El Hassani, A., Feist, R. & Hladil, J. 1997. Magnetosusceptibility event and cyclostratigraphy (MSEC) of the Eifelian-Givetian GSSP and associated boundary sequences in North Africa and Europe. *Episodes*, **20**, 167–175.

Crick, R. E., Ellwood, B. B., Hladil, J., El Hassani, A., Hrouda, F. & Chlupac, I. 2001. Magnetostratigraphy susceptibility of the Pridoli-Lochkovian GSSP (Klonk, Czech Republic) and a coeval sequence in Anti-Atlas Morocco. *Palaeogeography, Palaeoclimatology, Palaeoecology*, **167**, 73–100.

Crick, R. E., Drecsen, R. *et al.* 2002. Magnetostratigraphy susceptibility of the Frasnian/Famennian boundary. *Palaeogeography, Palaeoclimatology, Palaeoecology*, **181**, 67–90.

Da Silva, A. C. & Boulvain, F. 2006. Upper Devonian carbonate platform correlations and sea level variations recorded in magnetic susceptibility. *Palaeogeography, Palaeoclimatology, Palaeoecology*, **240**, 373–388.

Davis, J. C. 1986. *Statistics and Data Analysis in Geology*. John Wiley, Chichester, UK.

Dearing, J. A. 1999. Chapter 4. Magnetic Susceptibility. *In*: Walde, J., Oldfield, F. & Smith, J. (eds) *Environmental Magnetism: A Practical Guide*. Technical Guide, No. 6. Quaternary Research Association, London, 35–62.

Dercourt, J., Ricou, L. E. & Vrielynck, B. 1993. *Atlas Tethys Palaeoenvironmental Maps*. Gaulthier-Villars, Paris.

Dercourt, J., Gaetani, M. *et al.* 2000. *Atlas Peri-Tethys—Palaeogeographical Maps*. Commission of the Geological Map of the World, Paris.

Devleeschouwer, X. 1999. *La transition Frasnien-Famennien (Dévonien Supérieur) en Europe: Sédimentologie, stratigraphie séquentielle et susceptibilité magnétique*. PhD thesis, Université Libre de Bruxelles, Bruxelles, Belgium (in French).

Dubiel, R. F., Parrish, J. T., Parrish, J. M. & Good, S. C. 1991. The Pangean megamonsoon – evidence from the Upper Triassic Chinle Formation, Colorado Plateau. *Palaios*, **6**, 347–370.

Dumont, J. F. & Kerey, E. 1975. Kırkavak Fayı [The Kırkavak Fault]. *Türkiye Jeoloji Kurumu Bülteni [Bulletin of the Geological Society of Turkey]*, **18**, 59–62.

Dunlop, J. D. & Özdemir, Ö. 1997. *Rock Magnetism, Fundamentals and Frontiers*. Cambridge University Press, Cambridge.

Ellwood, B. B. & Ledbetter, M. T. 1977. Antarctic bottom water fluctuation in the Vema Channel: effects of velocity changes on particle alignment and size. *Earth and Planetary Science Letters*, **35**, 189–198.

Ellwood, B. B., Crick, R. E. & El Hassani, A. 1999. The magnetosusceptibility event and cyclostratigraphy (MSEC) method used in geological correlation of Devonian rocks from Anti-Atlas Morocco. *American Association of Petroleum Geologists Bulletin*, **83**, 1119–1134.

Ellwood, B. B., Crick, R. E., El Hassani, A., Benoist, S. L. & Young, R. H. 2000. Magnetosusceptibility event and cyclostratigraphy method applied to marine rocks: detrital input v. carbonate productivity. *Geology*, **25**, 1135–1138.

Ellwood, B. B., Crick, R. E., Garcia-Alcalde Fernandez, J.-L., Soto, F. M., Truyóls-Massoni, M., El Hassani, A. & Kovas, E. J. 2001. Global correlation using magnetic susceptibility data from Lower Devonian rocks. *Geology*, **29**, 583–586.

Ellwood, B. B., Brett, C. E., Tomkin, J. H. & MacDonald, W. D. 2013*a*. Visual identification and quantification of Milankovitch climate cycles in outcrop: an example from the Upper Ordovician Kope Formation, Northern Kentucky. *In*: Jovane, L., Herrero-Bervera, E., Hinnov, L. A. & Housen, B. A. (eds) *Magnetic Methods and the Timing of Geological Processes*. Geological Society, London, Special Publications, **373**, 341–353.

Ellwood, B. B., Lambert, L. L., Tomkin, J. H., Bell, G. L., Nestell, M. K., Nestell, G. P. & Wardlaw, B. R. 2013*b*. Magnetostratigraphy susceptibility for the Guadalupian series GSSPs (Middle Permian) in Guadalupe Mountains National Park and adjacent areas in West Texas. *In*: Jovane, L., Herrero-Bervera, E., Hinnov, L. A. & Housen, B. A. (eds) *Magnetic Methods and the Timing of Geological Processes*. Geological Society, London, Special Publications, **373**, 375–94.

Flügel, E. & Senowbari-Daryan, B. 2001. Triassic reefs of the Tethys. *In*: Stanley, G. D., Jr. (ed.) *The History and Sedimentology of Ancient Reef Systems*. Kluwer Academic/Plenum Publisher, New York, 217–249.

Gindl, A. 2000. *Paläoökologie triassischer Ammonitenfaunen des Taurusgebirges (Türkei)*. Unpublished Diploma thesis, University of Vienna.

Gradstein, F. M., Ogg, J. G. & Smith, A. G. 2004. *A Geologic Time Scale 2004*. Cambridge University Press, Cambridge.

Gutnic, M., Monod, O., Poisson, A. & Dumont, J. F. 1979. Géologie des Taurides Occidentales (Turquie). *Mémoire Societe Géologique de France*, **137**, 1–112.

Hagemeister, A. 1988. Zyklische Sedimentation auf einer stabilen Karbonatplattform: Die Raibler Schichten (Karn) des Drauzuges/ Kärnten (Österreich). *Facies*, **18**, 83–122.

Hallam, A. 1996. Major bio-events in the Triassic and Jurassic. *In*: Walliser, O. H. (ed.) *Global Events and Event-Stratigraphy*. Springer, Berlin, 265–283.

Hallam, A. & Wignall, P. B. 1997. *Mass Extinctions and their Aftermath*. Oxford University Press, Oxford.

Hammer, Ø. & Harper, A. T. 2006. *Paleontological Data Analysis*. Blackwell Publishing, Oxford, UK.

Hammer, Ø., Harper, A. T. & Ryan, P. D. 2008. PAST, Paleontological statistics. Version 1.87b, http://folk.uio.no/ohammer/past

HLADIL, J., GERSL, M., STRNAD, L., FRANA, J., LANGROVA, A. & SPISIAK, J. 2006. Stratigraphic variation of complex impurities in platform limestones and possible significance of atmospheric dust: a study with emphasis on gamma-ray spectrometry and magnetic susceptibility outcrop logging (Eifelian-Frasnian, Moravia, Czech Republic). *International Journal of Earth Sciences (Geologische Rundschau)*, **95**, 703–723.

HORNUNG, T. 2008. *The Carnian Crisis in the Tethys Realm.* Multistratigraphic Studies and Palaeoclimate Constraints. VDM Verlag Dr. Müller, Saarbrücken, 1–235.

HORNUNG, T. & BRANDNER, R. 2005. Biochronostratigraphy of the Reingraben Turnover (Hallstatt Facies Belt): local black shale events controlled by regional tectonics, climatic change and plate tectonics. *Facies*, **51**, 475–494.

HORNUNG, T., BRANDNER, R., KRYSTYN, L., JOACHIMSKI, M. & KEIM, L. 2007. Multistratigraphic constraints on the NW Tethyan 'Carnian crisis'. *In*: LUCAS, S. G. & SPIELMANN, J. A. (eds) *The Global Triassic*. New Mexico Museum of Natural History and Science Bulletin, Albuquerque, New Mexico, **41**, 59–67.

JERZ, H. 1966. Untersuchungen über Stoffbestand, Bildungsbedingungen und Paläogeographie der Raibler Schichten zwischen Lech und Inn (Nördliche Kalkalpen). *Geologia Bavarica*, **56**, 1–99.

JOVANE, L., HINNOV, L., HOUSEN, B. A. & HERRERO-BARVERA, E. 2013. Magnetic methods and the timing of geological processes. *In*: JOVANE, L., HERRERO-BERVERA, E., HINNOV, L. A. & HOUSEN, B. A. (eds) *Magnetic Methods and the Timing of Geological Processes*. Geological Society of London, Special Publications, **373**, 1–12.

KEIM, L., BRANDNER, R., KRYSTYN, L. & METTE, W. 2001. Termination of carbonate slope progradation: an example from the Carnian of the Dolomites, northern Italy. *Sedimentary Geology*, **143**, 303–323.

KODAMA, K. P. 2012. *Paleomagnetism of Sedimentary Rocks. Process and Interpretation*. Wiley-Blackwell, Chichester, UK.

KOZUR, H. W. & BACHMANN, G. H. 2010. The middle Carnian Wet Intermezzo of the Stuttgart Formation (Schilfsandstein), Germanic Basin. *Palaeogeography Palaeoclimatology Palaeoecology*, **290**, 107–119.

LAZAROFF, N. 1997. Mineral leaching, iron precipitation, and the sulfate requirement for chemolithotrophic iron oxidation. *In*: WISE, D. L. (ed.) *Global Environmental Biotechnology*. Springer-Verlag, Netherlands, 61–75.

LUKENEDER, S. & LUKENEDER, A. 2014. A new ammonoid fauna from the Carnian (Upper Triassic) Kasımlar Formation of the Taurus Mountains (Anatolia, Turkey). *Palaeontology*, **57**, 357–396, http://dx.doi.org/10.1111/pala.12070

LUKENEDER, A., HALÁSOVÁ, E. *ET AL.* 2010. High resolution stratigraphy of the Jurassic-Cretaceous boundary interval in the Gresten Klippenbelt (Austria). *Geologica Carpathica*, **5**, 365–381.

LUKENEDER, S., LUKENEDER, A., HARZHAUSER, M., ISLAMOGLU, Y., KRYSTYN, L. & LEIN, R. 2012. A delayed carbonate factory breakdown during the Tethyan-wide Carnian Pluvial Episode along the Cimmerian terranes (Taurus, Turkey). *Facies*, **58**, 279–296.

MONOD, O. 1977. *Recherches géologiques dans le Taurus Occidental au sud de Beyşehir (Turquie)*. PhD thesis, University of South Paris.

MUTTI, M. & WEISSERT, H. 1995. Triassic monsoonal climate and its signature in Ladinian-Carnian carbonate platforms (Southern Alps, Italy). *Journal of Sedimentary Research*, **B65**, 357–367.

OGG, J. G. 2012. Chapter 25. Triassic. *In*: GRADSTEIN, F. M., OGG, J. G., SCHMITZ, M. D. & OGG, G. M. (eds) *The Geological Time Scale*. Elsevier, Amsterdam, 681–730.

ÖZGÜL, N. & ARPAT, E. 1973. Structural units of Taurus orogenic belt and their continuation in the neighbouring regions. *Geological Society of Greece Bulletin*, **10**, 156–164.

PARRISH, J. T. 1993. Climate of the supercontinent Pangea. *Journal of Geology*, **101**, 215–233.

PARRISH, J. T. & PETERSON, F. 1988. Wind directions predicted from global circulation models and wind directions determined from eolian sandstones of the western United States – a comparison. *Sedimentary Geology*, **56**, 261–282.

POISSON, A. 1977. *Recherches géologiques dans les Taurides occidentals (Turquie)*. PhD thesis, University of South Paris.

PRETO, N., KUSTATSCHER, E. & WIGNALL, P. B. 2010. Triassic climates – State of the art and perspectives. *Palaeogeography, Palaeoclimatology, Palaeoecology*, **290**, 1–10.

RACKI, G., RACKA, M., MATYJA, H. & DEVLEESCHOUWER, X. 2002. The Frasnian/Famennian boundary interval in the South Polish-Moravian shelf basins: integrated event-stratigraphical approach. *Palaeogeography, Palaeoclimatology, Palaeoecology*, **181**, 251–297.

RICHTHOFEN, F. V. 1860. *Geognostische Beschreibung der Umgebung von Predazzo, Sanct Cassian und der Seisser Alpe in Süd Tyrol*. Justus Perthes Verlag, Gotha.

RIDER, H. 1990. Gamma-ray log shape used as a facies indicator: critical analysis of an oversimplified methodology. *In*: HURST, A., LOVELL, M. A. & MORTON, A. C. (eds) *Geological Applications of Wireline Logs*. Geological Society, London, Special Publications, **48**, 27–37.

RIEDEL, P. 1991. Korallen in der Trias der Tethys: Stratigraphische Reichweiten, Diversitätsmuster, Entwicklungstrends und Bedeutung als Rifforganismen. *Mitteilungen der Gesellschaft der Geologie- und Bergbaustudenten*, **37**, 97–118.

ROBERTSON, A. H. F. 1993. Mesozoic-Tertiary sedimentary and tectonic evolution of Neotethyan carbonate platforms, margins and small ocean basins in the Antalya Complex, southwest Turkey. *International Association of Sedimentologists, Special Publications*, **20**, 415–465.

ROBERTSON, A. H. F. 2000. Mesozoic-Tertiary tectonic-sedimentary evolution of a south Tethyan Oceanic Basin and its margins in southern Turkey. *In*: BOZKURT, E., WINCHESTER, J. A. & PIPER, J. D. A. (eds) *Tectonics and Magmatism in Turkey and the Surrounding Area*. Geological Society of London, Special Publications, **173**, 97–138.

ROBERTSON, A. H. F., POISSON, A. & AKINCI, Ö. 2003. Developments in research concerning Mesozoic-Tertiary Tethys and neotectonics in the Isparta Angle, SW Turkey. *Geological Journal*, **38**, 195–234.

ROBINSON, S. G. 1973. Paleoclimatology and continental drift. *In*: TARLING, D. H. & RUNCORN, S. K. (eds) *Implications of Continental Drift to the Earth Sciences*. Academia Press, London, 449–476.

ROBINSON, S. G. 1990. Applications for whole core magnetic susceptibility measurements of deep-sea sediments. Leg 115 results. *Proceedings of the Ocean Drilling Program, Scientific Results*, **115**, 737–771.

RÜFFER, T. & ZAMPARELLI, V. 1997. Facies and biota of Anisian to Carnian carbonate platforms in the Northern Calcareous Alps (Tyrol and Bavaria). *Facies*, **37**, 115–136.

SCHULER, 1968. Lithofazielle, sedimentologische u. paläogeographische Untersuchungen in den Raibler Schichten zwischen Inn und Saalach (Nördliche Kalkalpen). *Erlanger Geologische Abhandlungen*, **71**, 1–60.

SCOTESE, C. R. 1998. *Quicktime Computer Animations*. PALEOMAP Project, Department of Geology. University of Texas at Arlington, Arlington.

SCOTESE, C. R. 2001. *Paleomap Project*, http://www.scotese.com/

SCOTESE, C. R., GAHAGAN, L. M. & LARSON, R. L. 1989. Plate tectonic reconstructions of the Cretaceous and Cenozoic ocean basins. *In*: SCOTESE, C. R. & SAGER, W. W. (eds) *Mesozoic and Cenozoic Plate Reconstructions*. Elsevier, Amsterdam, 27–48.

SENEL, M. 1997. *Geological map of Turkey. Nr. 4, Isparta Paftasi*. Department of Geology, Ankara, 1–23.

ŞENGÖR, A. M. C., YILMAZ, Y. & SUNGURLU, O. 1984. Tectonics of the Mediterranean Cimmerids: nature and evolution of the western termination of Palaeo-Tethys. *In*: DIXON, J. E. & ROBERTSON, A. H. F. (eds) *The Geological Evolution of the Eastern Mediterranean*. Geological Society, London, Special Publications, **17**, 77–112.

SERRA, O. 1984. *Fundamentals of Well-Log Interpretation (Vol. 1): The Acquisition of Logging Data. Developments in Petroleum Science. 15A*. Elsevier, Amsterdam.

SERRA, O., BALDWIN, J. & QUIREIN, J. 1980. Theory, interpretation and practical applications of natural gamma ray spectroscopy. *Society of Petrophysicists and Well Log Analysts (SPWLA), 21st Annual Logging Symposium, 8th–11th July, Lafaette, Louisiana*, **27**, Q1–Q30.

SIMMS, M. J. & RUFFELL, A. H. 1989. Synchronicity of climate change and extinctions in the Late Triassic. *Geology*, **17**, 265–268.

STAMPFLI, G. M. & BOREL, G. D. 2002. A plate tectonic model for the Paleozoic and Mesozoic constrained by dynamic plate boundaries and restored synthetic oceanic isochrons. *Earth and Planetary Science Letters*, **196**, 17–33.

STAMPFLI, G. M., BOREL, G. D., MARCHANT, R. & MOSAR, J. 2002. Western Alps geological constraints on western Tethyan reconstructions. *Journal of the Virtual Explorer*, **8**, 77–106.

TOLLMANN, A. 1976. *Analyse des klassischen nordalpinen Mesozoikums: Stratigraphie, Fauna und Fazies der Nördlichen Kalkalpen*. Monographie der Nördlichen Kalkalpen 2. Franz Deuticke, Wien.

WHALEN, M. T. & DAY, J. E. 2010. Cross-basin variations in magnetic susceptibility influenced by changing sea level, paleogeography, and paleoclimate: Upper Devonian, Western Canada sedimentary basin. *Journal of Sedimentary Research*, **80**, 1109–1127.

ZHANG, S., WANG, X. & ZHU, H. 2000. Magnetic susceptibility variations of carbonates controlled by sea level changes. Examples in Devonian to Carboniferous strata in southern Guizhou Province, China. *Science in China D, Earth Sciences*, **43**, 266–276.